Multiple poliovirus-induced organelles suggested by comparison of spatiotemporal dynamics of membranous structures and phosphoinositides

Hyung S. Oh[1], Sravani Banerjee[1], David Aponte-Diaz, Jason Aligo[2], Maria F. Lodeiro and Craig E. Cameron*

Department of Biochemistry and Molecular Biology, The Pennsylvania State University, University Park, PA 16802

[1]These authors contributed equally to this study.

[2]Current address: Biologics Toxicology, Janssen Research and Development, LLC, Spring House, PA 19477

*Correspondence: cec9@psu.edu; 814-863-8705 (Phone); 814-863-7024 (Fax); @CameronLabPSU (Twitter)

Running Title: Multiple PV-induced organelles

ABSTRACT

Poliovirus (PV) infection induces membranes with elevated levels of phosphatidylinositol-4-phosphate (PI4P) and invaginated, tubular structures that appear as vesicular clusters in cross section. Here, we characterize PV mutants, termed EG and GG, which exhibit aberrant proteolytic processing of the P3 precursor that can delay the onset of genome replication and/or impair virus assembly. For WT PV, changes to the PI4P pool were observed as early as 30 min post-infection. PI4P remodeling occurred even in the presence of guanidine hydrochloride, a replication inhibitor. Vesicular clusters were not apparent until 3 h post-infection, a time too slow for these structures to be responsible for genome replication. Delays in the onset of genome replication observed for EG and GG PVs were explained completely by the reduced kinetics of virus-induced remodeling of PI4P pools, consistent with PI4P serving as a marker of the genome-replication organelle. Infectious virus produced by GG PV is known to be reduced nearly 5-logs. We show that GG PV was unable to make virus-induced vesicular clusters. Instead, GG PV-infected cells accumulated elongated tubules. Our results are consistent with the existence of distinct organelles for genome replication and virus assembly. We suggest that the pace of formation and spatiotemporal dynamics of PV-induced organelles may be set by the rate of P3 precursor processing to form 3AB and/or 3CD proteins.

AUTHOR SUMMARY – All positive-strand RNA viruses replicate their genomes in association with host cell membranes. PV does not just remodel existing membranes, but induces membranes with unique structure and lipid composition. There has been some suggestion that the functions of the PV-induced structures observed during infection may not be those that perform genome replication. This study uses kinetic analysis of virus-induced membrane formation and PI4P induction by two PV mutants to provide evidence for the existence of a virus-induced genome-replication organelle distinct from a second organelle, the absence of which impairs virus assembly. In addition, our studies suggest that formation of both organelles may require participation of viral proteins, 3AB and/or 3CD. Therefore, this study provides a new perspective on the cell biology of PV infection and should inspire a fresh look at picornavirus-induced organelles, their functions and the role of P3 proteins in their formation.

INTRODUCTION

Positive-strand RNA viruses pose a great threat to public health because of their simplicity and evolvability [1]. Introduction of a modestly-sized, mRNA-sense genome is sufficient to commandeer the cell, establish infection and produce thousands of progeny in a matter of only hours. Among the least understood aspect of positive-strand RNA virus biology is the eclipse phase of the life cycle, the events post-entry but prior to exponential amplification of the genome and assembly of infectious virus. We use poliovirus (PV), the type virus in the Enterovirus genus of the *Picornaviridae* family of viruses, as our model system. Establishment of infection by PV likely requires entry of multiple genomes into the cell [2, 3]. This circumstance may be required to permit translation of infecting virion RNA to produce viral protein in sufficient quantity to overwhelm host defenses that might otherwise curtail infection and to hijack host factors essential to initiate a productive infection. It is becoming increasingly clear that picornaviruses have evolved mechanisms to increase multiplicity of infection, for example by leaving cells in vesicles and perhaps entering that way [4] or by attaching to bacterial surface polysaccharides and entering in association with these organisms [5].

Another important function of viral proteins produced during the eclipse phase is establishment of sites of genome replication. All positive-strand RNA viruses replicate in association with membranes; three general strategies exist [6]. The first strategy is to commandeer an organellar membrane by directing viral proteins to the organelle. Binding of the viral protein will induce invaginations with negative curvature from the perspective of the cytoplasm that have been termed spherules. In response to actions of the same or different viral proteins, the lipid and protein composition of the spherules may be remodeled to reflect the genome-replication needs of the virus. The second strategy uses a two-step process. The virus commandeers vesicular and/or organellar membranes, again by directing viral proteins to their membranes. Hijacked membranes are then forced into a new form by remodeling lipid and/or protein composition to create a virus-induced organelle best suited to genome replication. The third strategy is a blend of the first two. Localize first to an organelle and later induce a virus-specific organelle(s), which may be the case for enteroviruses [7].

Since the earliest studies of PV-infected cells using transmission electron microscopy (TEM), it has been well documented that PV infection wreaks havoc on intracellular membranes, for example causing dissolution of the Golgi apparatus (referred to throughout as Golgi), to create membranes of unique benefit to the virus [8-12]. PV-induced membranes often appear as clusters of vesicles by TEM. These structures have been shown to contain viral RNA and proteins [13-16]. More recent studies by Ehrenfeld, Belov and colleagues using electron tomography have suggested that PV-induced membranes arise from

60 tubules [9]. The thought is that viral or viral-hijacked proteins induce invaginations of positive curvature
61 and promote folding of tubules, which would appear as vesicular clusters in cross section. In the Ehrenfeld
62 and Belov study, a kinetic analysis was performed that provided the first suggestion that the most
63 dramatic PV-induced changes to membranes occurred after genome-replication was well underway, if not
64 completed.

65 Prior to the tomography study, Altan-Bonnet and colleagues showed induction of
66 phosphatidylinositol-4-phosphate (PI4P) by another member of the Enterovirus genus, Coxsackievirus B3
67 (CVB3) [17]. In uninfected cells, PI4P localizes to the Golgi. During infection, PI4P starts at the Golgi then
68 relocalizes to a site between the endoplasmic reticulum (ER) and Golgi, perhaps the ER-Golgi intermediate
69 compartment (ERGIC). At later times post-infection, PI4P fills the entire perinuclear region of the cell and
70 now localizes with ER markers. During the entire infection period, PI4P localizes with viral RNA and
71 proteins. One conclusion of the study was that PI4P is a marker of the PV-induced organelle. When
72 considered in the context of the tomography study, it is possible that the perinuclear PI4P observed for
73 CVB3 reflects the invaginated and folded tubules observed for PV that might not function in genome
74 replication. Therefore, the earliest stages of PI4P induction and membrane remodeling may actually
75 represent the replication organelle, for which TEM images are not available.

76 The large polyprotein encoded by the PV genome can be divided into three smaller precursor
77 proteins: P1, P2 and P3 (**Fig. 1A**) [18]. P1 proteins form the capsid. P2 proteins are thought to be the
78 most functionally diverse of the PV proteins as these proteins shut off host cell pathways, derange host
79 cell membranes, function in genome replication and genome encapsidation, and can even leave their
80 mark on the encapsidated genome by somehow controlling its uncoating [12, 14, 19-30]. P3 proteins are
81 most intimately associated with genome replication as these proteins bind to the genome and catalyze
82 RNA synthesis [31-37].

83 PV uses differential cleavage of the polyprotein as one mechanism to expand its proteome.
84 Cleavage of the P3 precursor protein is mediated by the 3C-encoded protease activity. This protease
85 cleaves at Gln-Gly junctions, but the requirements for cleavage extend beyond a single dipeptide [38-40].
86 Two pathways exist for cleavage of P3 [41, 42]. The major pathway produces only two proteins: 3AB and
87 3CD (**Fig. 1B**). The minor pathway is more complex. First, P3 is cleaved to produce 3A and 3BCD proteins.
88 3BCD is then cleaved to produce 3BC and 3D. Finally, 3BC is cleaved to produce 3B (also known as VPg,
89 virion protein linked to the genome) and 3C.

90 Previously, we reported two PV mutants in which the cleavage site between 3B and 3C was
91 changed to Gly-Gly (GG PV) [42] or Glu-Gly (EG PV) [42, 43]. For GG PV, the products of the major pathway

92 were 3ABC and 3D, thus ablating the production of both 3AB and 3CD (see GG in **Fig. 1B**). With the
93 exception of 3BC, which cannot be cleaved, products of the minor pathway were essentially unchanged
94 [42]. For EG PV, the products of both pathways were the same as observed for wild type (see EG in **Fig.**
95 **1B**). However, the rate of cleavage at the 3BC junction was reduced, causing a reduced rate of
96 accumulation of 3AB and 3CD. Both mutants exhibited what appeared to be a reduced rate of genome
97 replication. For EG PV, ectopic expression of 3CD alone corrected this phenotype, consistent with the
98 phenotype arising solely from the reduced rate of 3CD production. In addition to the impact on genome
99 yield, GG PV exhibited a near-complete loss of infectious virus. Neither of the GG PV phenotypes could
100 be suppressed by ectopic expression of 3CD.
101 The extended duration of the eclipse phase observed for EG PV and the defect to virus assembly
102 observed for GG PV provided a unique opportunity to expand our understanding of these steps of the
103 virus lifecycle at the molecular and ultrastructural levels. We find that there is a clear temporal ordering
104 of PI4P induction and its initial induction and limited redistribution exhibit the expected kinetics for an
105 organelle involved in genome replication. During the early stages of PI4P remodeling, Golgi fragments
106 and ERGIC expands. It is only after genome replication is near completion that the perinuclear region of
107 the cell becomes filled with vesicular clusters. At the same stage of genome replication that vesicular
108 clusters predominate for WT PV, tubules predominate for GG PV. The inability of GG PV to assemble
109 infectious virus is consistent with the possibility that vesicular clusters contribute substantively to steps
110 after genome replication on path to production of infectious virus. We propose that two organelles are
111 induced during PV infection that serve distinct functions during the PV lifecycle and that P3-encoded
112 proteins contribute to formation and function of both.
113
114

115 **RESULTS**

116 **Delayed release of 3AB and 3CD proteins from the P3 precursor protein delays onset of genome**
117 **replication.**

118 Our previous studies of EG PV showed that its genome-replication defect could be complemented
119 in trans by expression of 3CD [43]. This observation was unexpected because numerous studies have
120 shown that genome-replication defects can only be complemented in trans by expression of P3 or P2-P3
121 polyproteins, if at all [44-46]. Our study used a subgenomic replicon in which P1-coding sequence had
122 been replaced with firefly luciferase-coding sequence, and replication was monitored indirectly by
123 measuring luciferase activity. It was possible that measuring luciferase activity instead of RNA confounded
124 our interpretation of the experiment.

125 To test this possibility, we transfected WT or EG PV subgenomic replicon RNA into HeLa cells. We
126 monitored RNA synthesis either by measuring luciferase activity (**Fig. 2A**) or by measuring positive-sense
127 RNA using Northern blotting (**Figs. 2B and 2C**). We observed three discernible phases of luciferase activity
128 for WT: 0-2 h, 2-5 h, and 5-10 h; and for EG: 0-3 h, 3-7 h and 7-10 h (**Fig. 2A**). In contrast, we observed
129 only one phase of RNA accumulation for both (**Fig. 2B**). WT RNA accumulation began between 1-2 h post-
130 transfection; EG RNA accumulation began between 3-4 h post-transfection (**Fig. 2B**). We conclude that a
131 delay of two hours in the onset of replicon RNA replication can be obscured by monitoring luciferase
132 activity. Luciferase activity concealed the delay. Translation of transfected replicon RNA produced
133 luciferase activity for at least two hours in the presence of guanidine hydrochloride (GuHCl), a replication
134 inhibitor, and therefore without the need for replicon RNA replication (see WT +GuHCl in **Fig. 2A**). These
135 results support the hypothesis that delayed kinetics of P3 precursor processing to form 3AB and 3CD in
136 cells causes a delay in a step preceding the onset of RNA synthesis.

137 **Kinetics of formation of PV-induced vesicular clusters are inconsistent with these structures serving as**
138 **the sites of genome replication.**

139 A hallmark of PV-infected cells as observed by transmission electron microscopy (TEM) is the
140 presence of vesicular clusters [9, 12]. These vesicular clusters are also referred to as replication complexes
141 or replication organelles. Given the accepted role of these vesicular clusters in genome replication, we
142 reasoned that formation of these structures should occur either prior to the onset of genome replication
143 or concomitant with genome replication. Formation and/or function of these structures could therefore
144 represent the pre-genome-replication step perturbed for EG PV.

145 We infected HeLa cells with EG PV and then at various times post-infection processed samples to
146 measure genomic RNA by Northern blotting (**Figs. 3A** and **3B**), to measure infectious virus by plaque assay

147 (**Fig. 3A**) and to visualize formation of the vesicular clusters by TEM (**Fig. 3C**). The exponential phase of
148 genome replication occurred between 2 h and 6 h post-infection (**Figs. 3A** and **3B**). The exponential phase
149 of infectious virus production occurred between 4 h and 8 h post-infection (**Fig. 3A**). Vesicular clusters
150 became visible at 4 h post-infection and continued to increase in abundance and/or change in organization
151 throughout the 7 h time course (**Fig. 3C**). Formation of vesicular clusters neither preceded genome
152 replication nor occurred concomitant with genome replication as expected for an organelle responsible
153 for genome replication. In contrast, formation of vesicular clusters preceded infectious virus production.
154 The delay in induction of the vesicular clusters by EG PV provided a unique opportunity to monitor
155 the early steps in formation of these structures. In uninfected cells, it was very easy to observe
156 mitochondria and Golgi. However, closer inspection was required to observe the tubules of the
157 endoplasmic reticulum (ER) (uninfected in **Fig. 3C**). By 2 h post-infection, the density of mitochondria had
158 diminished (2 h in **Fig. 3C**). Golgi stacks were fragmented and swollen, and the tubules of the ER and/or
159 ER-Golgi intermediate compartment (ERGIC) were swollen and easier to visualize (2 h in **Fig. 3C**). At 3 h
160 post-infection, much of the Golgi had disappeared (3 h in **Fig. 3C**). The area between the remaining Golgi
161 and the now very swollen ER was filled with very small vesicles that may be the ever-expanding ERGIC
162 caused by the loss of the Golgi (3 h in **Fig. 3C**) [17]. At 4 h post-infection, vesicular clusters were first
163 observed (4 h in **Fig. 3C**). These vesicular clusters appear to be encased by the swollen tubules of the ER
164 (4 h in **Fig. 3C**).
165 In order to make certain that our observations above were not unique to the mutant virus, we
166 repeated the experiment using WT PV (**Fig. 4**). The exponential phase of genome replication occurred
167 between 1 h and 5 h post-infection (**Figs. 4A** and **4B**). The exponential phase of infectious virus production
168 occurred between 3 h and 7 h post-infection (**Fig. 4A**). Vesicular clusters were now clearly visible at 3 h
169 post-infection and again continued to increase in abundance or change in organization throughout the 7
170 h time course (**Fig. 4C**). Many of the early steps described for EG PV could not be observed for wild type
171 because they occurred so soon post-infection that we could not process the cells fast enough to capture
172 images of these steps by TEM.
173 In addition to the temporal difference in the formation of the vesicular clusters observed for EG
174 PV and WT PV, differences also existed in the overall size, interaction and localization of these structures
175 (compare 5 h for EG PV in **Fig. 3C** to 4 h for WT PV in **Fig. 4C**). Relative to EG PV, vesicular clusters induced
176 by WT PV appeared larger, clustered more tightly and were far more constrained to the perinuclear region
177 of the cell.

178 Both experiments were consistent with the surprising finding that the kinetics of formation of the
179 PV-induced vesicular clusters are inconsistent with these structures serving as the genome-replication
180 organelle. These structures became easily identifiable two hours after genome replication began (4 h for
181 EG PV in **Fig. 3C**; 3 h for WT PV in **Fig. 4C**). Interestingly, and perhaps coincidentally, this was the time
182 after genome replication began that we were able to detect infectious virus by plaque assay (**Figs. 3B** and
183 **4B**).

184 **Kinetics of PI4P induction are consistent with this phosphoinositide demarcating the sites of genome**
185 **replication.**

186 Coxsackievirus B3 (CVB3) infection induces PI4P and this phosphoinositide is a component of a
187 virus-induced organelle [17]. PI4P co-localizes with viral non-structural proteins and RNA [17]. Whether
188 or not PI4P localizes to the virus-induced vesicular clusters is not known. Given our results, it is possible
189 that the virus-induced PI4P localizes to membranes other than those observed by TEM well after genome
190 replication has begun.

191 Although it is assumed that PV infection induces PI4P based on the data for CVB3, PI4P induction
192 by PV has never been reported. We infected HeLa cells with WT PV or EG PV and measured PI4P as a
193 function of time post-infection by immunofluorescence microscopy (IFM) (**Fig. 5**). We used an antibody
194 specific for PI4P to detect this phosphoinositide.

195 It is well known that most PI4P in the cell localizes to the Golgi, giving rise to very nice staining
196 with anti-PI4P antibody (mock in **Fig. 5A**) [17]. For WT PV, induction and redistribution of Golgi-localized
197 PI4P was evident as early as 30 min post-infection WT in **Fig. 5B**). Both redistribution and induction
198 continued to 3 h post-infection, the last time point evaluated (WT in **Fig. 5B**). Observations with EG PV
199 were essentially identical, except for a one-hour delay of the changes relative to wild type (EG in **Fig. 5B**).
200 The kinetics of induction and redistribution of PI4P were consistent with a structure responsible for
201 genome replication. Given the TEM experiments reported above (**Figs. 3** and **4**), it is now clear that the
202 PI4P-containing membranes observed by IFM prior to two hours post-infection (**Fig. 5B**) must be distinct
203 from the large vesicular clusters that appear after genome replication (**Figs. 3** and **4**).

204 PI4P induction and redistribution during WT PV infection occurred as fast as we could reliably
205 process our cells for imaging. This observation suggested to us that viral proteins made by translation of
206 infecting viral RNA might be sufficient to initiate PI4P remodeling. We infected cells with WT or EG PV in
207 the presence of the genome-replication inhibitor, GuHCl. Under these conditions, the only event that can
208 occur is translation of the infecting genomes. PI4P induction and redistribution occurred in the presence

209 of GuHCl for both WT (WT+GuHCl in **Fig. 5C**) EG (EG+GuHCl in **Fig. 5C**) PVs. GuHCl did not have an impact
210 on PI4P localization in the absence of infection (Mock+GuHCl in **Fig. 5C**).

211 **PV-induced vesicular clusters as sites of virus assembly, an assembly organelle?**

212 The studies reported above suggested that PI4P was a marker for the PV genome-replication
213 organelle. These studies also suggested that PI4P-containing structures observed early are distinct from
214 PV-induced vesicular clusters. The question now was: what is the function of the vesicular clusters? One
215 possibility was that the vesicular clusters are structures required for virus assembly, an assembly
216 organelle, as suggested previously by Belov and Ehrenfeld [9]. Another possibility was that the vesicular
217 clusters are structures that represent accumulated, unused and unwanted viral proteins and nucleic acids,
218 a viral trash compacter.

219 GG PV replicated to within one log of wild type but exhibited a near 5-log reduction in the amount
220 of infectious virus produced [42]. We reasoned that this mutant might help us identify the function of the
221 PV-induced vesicular clusters. If the vesicular clusters contribute to virus assembly, then these structures
222 might be perturbed in cells infected with the assembly-defective GG PV. Conversely, if the vesicular
223 clusters function as a means to consolidate viral waste, then these structures might appear unchanged in
224 cells infected with GG PV.

225 We transfected HeLa cells simultaneously with two subgenomic replicons, one expressing
226 luciferase and the other expressing EGFP. Transfected cells were then grown in suspension culture and
227 harvested hourly to monitor luciferase activity and EGFP fluorescence. Luciferase specific activity,
228 measured as relative light units per microgram of protein in the extract, was plotted as a function of time
229 for WT and GG replicons (**Fig. 6A**). We were particularly interested in 5 h post-transfection for WT as
230 vesicular clusters reached their maximum level at that time (**Fig. 4C**). At 5 h post-transfection of the WT
231 replicon combination, the luciferase specific activity was approximately 10^4 RLU/µg (**Fig. 6A**). We
232 observed the equivalent luciferase specific activity at 14 h post-transfection of the GG replicon
233 combination (**Fig. 6A**). Based on this result, we concluded that 5 h and 14 h post-transfection represented
234 equivalent extents of the infection process for WT and GG PVs, respectively.

235 We used fluorescence activated cell sorting (FACS) to isolate transfected cells based on EGFP
236 expression. Cells replicating WT or GG EGFP-replicon RNA before and after sorting are shown in **Fig. 6B**.
237 We used the EGFP-expressing, sorted cells for TEM (**Fig. 6C**). Vesicular clusters were readily apparent in
238 images of WT replicon-transfected cells, and these clusters were of the same overall appearance as
239 observed using infected cells that did not require sorting (**Fig. 4C**). In contrast, vesicular clusters were few

240 or absent in images of GG replicon-transfected cells (**Fig. 6C**). Instead, we observed a tubular/reticular
241 network (see enlargement of panel GG in **Fig 6C**).

242 These results support the hypothesis that vesicular clusters function as an assembly organelle,
243 and the absence of these structures in GG PV contribute to the defect in virus production. We propose
244 that the tubular/reticular network is an intermediate on the pathway to formation of the vesicular
245 clusters. These structures were apparent between 2 h and 4 h post-infection for EG PV (**Fig. 3C**) but
246 occurred too early to be observed for WT PV (**Fig. 4C**). The tubules appeared to fold in on themselves,
247 creating the vesicular clusters (see for example 4 hpi for EG PV in **Fig. 3C** or 3 hpi for WT PV in **Fig. 4C**).
248 Formation of tubules and their transformation into a net-like array of vesicles has been observed before
249 [9]. Additional studies will also be required to further clarify the relationship between the
250 tubular/reticular network in GG PV and the vesicular clusters in EG PV and WT PV.

251 Finally, we assessed formation of the PI4P-marked structures by GG PV RNA. We transfected HeLa
252 cells with GG PV EGFP-expressing, subgenomic replicon RNA and used IFM to monitor the spatiotemporal
253 dynamics of PI4P. Redistribution and induction of PI4P occurred substantially slower than observed for
254 EG PV or WT PV (compare **Fig. 6D** to **Fig. 5**). Nevertheless, temporal dynamics of PI4P explains the 8 h or
255 so pre-genome-replication phase observed previously for GG PV [42, 43]. These data are consistent with
256 PI4P demarcating the replication organelle and a requirement for induction of this structure prior to the
257 onset of genome replication.

258 **High multiplicity of infection exaggerates spatiotemporal dynamics of vesicular clusters.**

259 The spatiotemporal dynamics of WT PV-induced vesicular clusters reported here were different
260 than observed previously by others [9, 11, 16]. In particular, formation of the clusters was slower, and
261 the density of the clusters was lower (**Fig. 4C**) than previously reported. In these earlier experiments,
262 multiplicity of infection ranged from 30-50, but this study used 10. Because translation of the infecting
263 genomes is sufficient to begin the remodeling process, it was possible that elevated levels of protein
264 produced at the higher multiplicities of infection might impact the size of the clusters. To address this
265 possibility, we infected HeLa cells with WT PV at a multiplicity of 10, 50 or 100 and processed the infected
266 cells for TEM at 3 h post-infection. This time point was chosen because of the modest density of the
267 vesicular clusters observed at a multiplicity of infection of 10 (**Fig. 4C**) and should make any observed
268 differences more noticeable. As shown in **Fig. 7**, the size of the vesicular cluster at the level of each
269 "vesicle" and in terms of the area of the perinuclear region occupied by the vesicular clusters scaled
270 directly with the multiplicity of infection. Therefore, it is imperative to consider multiplicity of infection
271 when comparing micrographs.

272 **DISCUSSION**

273 This study was inspired by our observation that ectopic expression of PV 3CD protein was
274 sufficient to complement a genome-replication defect of the EG PV mutant, which exhibited a delay in
275 processing of the P3 precursor protein [43]. The rule of thumb for PV and other picornaviruses is that
276 non-structural proteins used to replicate a genome are produced in cis—that is, by that genome or by one
277 in the same replication complex [44-46]. However, it became clear that the genome-replication defect
278 was actually a defect at steps preceding genome replication (**Fig. 2B**). The confusion was caused by the
279 multiphasic kinetics of reporter activity produced by a subgenomic replicon (**Fig. 2A**). The first phase of
280 activity requires only translation of the transfected replicon. The second phase requires replicon
281 replication. The third phase appears to be translation of replicated replicon RNA that would normally be
282 packaged if capsid proteins had been present.

283 Once we knew that EG PV impaired steps leading up to genome replication, we turned our focus
284 to formation of the "replication organelle." Since the first TEM images of PV-infected cells were published
285 [8], multiple reports have shown that a hallmark of PV infection is the induction of membranous structures
286 [9-12]. These structures have many names: replication complexes, vesicular clusters, tubules and
287 replication organelle. Most of the early studies searching for viral factors contributing to formation of PV-
288 induced membranes implicated P2 proteins in this process [14, 15]. The most convincing experiment
289 showed that expression of the 2BC precursor proteins was sufficient to induce membranes with the same
290 buoyant density and appearance by TEM as those observed during PV infection [20, 21]. As a result, it
291 was unclear how processing of the P3 precursor to form 3AB and 3CD contributed to formation of the
292 replication organelle. However, because formation of this structure should precede genome replication,
293 it was possible that this step could be complemented in trans. 3A is known to inhibit guanine nucleotide
294 exchange factor (GEF), GBF1, which prevents trafficking between ER and Golgi and thereby causes
295 dissolution of the Golgi [47-52]. 3AB might also have this activity. Inhibition of ER-to-Golgi trafficking
296 should enlarge the ER-Golgi intermediate compartment, and this compartment has been implicated in
297 genome replication [17, 51]. 3AB is also known to promote invagination of membranes, an activity that
298 could contribute to formation of vesicular clusters [53]. 3CD, on the other hand, has not been shown to
299 perturb membrane form or function in cells. However, in cell-free extracts, the presence of 3CD promotes
300 recruitment of ADP-ribosylation factors (ARFs) and GEFs to membranes, which could modulate vesicular
301 trafficking and/or fusion [54, 55].

302 Our examination of the kinetics of formation of the vesicular clusters by EG PV relative to the
303 kinetics of genome replication was eye-opening. The kinetics of these two processes did not have the

304 expected behavior---that is, the site of RNA synthesis forming prior to RNA synthesis (**Fig. 3**). This
305 unexpected kinetic behavior was not an oddity of the mutant as WT PV also exhibited this behavior (**Fig.**
306 **4**). Our conclusion was that the vesicular clusters must not be the replication organelle. Belov and
307 Ehrenfeld floated this possibility several years ago [9]. In reviewing the literature on formation of PV-
308 induced vesicles, it became clear that the TEM images of others showed faster formation of vesicular
309 clusters in spite of the fact that kinetics of genome replication and/or production of infectious virus were
310 identical [9, 11, 16]. The one difference between our study and those of others was the multiplicity of
311 infection used. We used an MOI of 10 pfu/cell; others used an MOI of 30-50 pfu/cell. When we increased
312 the MOI to these higher levels, we observed faster kinetics of formation of the vesicular clusters (**Fig. 7**).
313 Under these conditions, the vesicular clusters were also substantially larger (**Fig. 7**). These observations
314 suggest that the kinetics of vesicular cluster formation can be modulated by multiplicity of infection
315 without a concomitant increase in the kinetics of genome replication or virus assembly, thus creating
316 some ambiguity to the temporal ordering of formation of the vesicular clusters relative to replication of
317 the genome.

318 Altan-Bonnet and colleagues showed that phosphatidylinositol-4-phosphate (PI4P) is induced by
319 Coxsackievirus B3 infection and redistributes from the Golgi to sites thought to be involved in genome
320 replication [17]. Therefore, we monitored the spatiotemporal dynamics of PI4P during PV infection. We
321 found that the spatiotemporal dynamics of the PI4P pool was completely consistent with PI4P
322 demarcating the replication organelle as induction and redistribution occurred well before the onset of
323 genome replication (**Fig. 5A**). Moreover, spatiotemporal dynamics of PI4P was delayed for EG PV (**Fig.**
324 **5B**). Unexpectedly, PI4P induction and redistribution did not require any genome replication as these
325 events occurred in the presence of a replication inhibitor. To the best of our knowledge, this observation
326 is among the first to link translation of infecting viral genomes alone to events essential for genome
327 replication. Under these conditions, the amount of viral proteins produced cannot be detected readily by
328 Western blotting or immunofluorescence [42, 43]. Therefore, very little of one or more viral proteins is
329 sufficient to hijack cellular factors needed for PI4P induction and redistribution.

330 We propose that 3AB and/or 3CD contribute to PI4P induction and/or redistribution. If this is the
331 case, then delays in P3 processing would be expected to have an impact on PI4P dynamics. Our initial
332 characterization of EG PV showed that its genome-replication phenotype could be complemented fully by
333 ectopic expression of 3CD [43]. It is therefore possible that 3CD or 3CD-containing precursor alone
334 contribute to PI4P dynamics. Interestingly, synthesis of PI4P by the beta isoform of the class III
335 phosphatidylinositol-4-kinase (PI4KIIIβ), the isoform thought to be responsible for induction of PI4P by

336 enteroviruses [17], is known to require Arf1 and GBF1 [17]. Perhaps the ability of 3CD to induce
337 translocation of Arf1 and GBF1 from the cytoplasm to membranes may be related to its role in PI4P
338 induction suggested here [54, 55].

339 The delay in formation of the replication organelle by EG PV created a window into the early
340 events of this process. It was possible to visualize Golgi fragmentation, proliferation of vesicles in the area
341 between ER and Golgi, and formation of short, thick tubules (**Fig. 3**). These events were suggested by
342 Altan-Bonnet and colleagues based on Golgi, ERGIC and ER marker co-localization with PI4P and CVB3
343 non-structural proteins and/or RNA [17]. Together, these data make a compelling case for these localized
344 membranous structures including and between ER and Golgi representing the replication organelle.

345 Clues into the formation and function of PV-induced vesicular clusters were obtained from studies
346 of GG PV. This mutant took even longer to initiate genome replication than EG PV, and this delay was
347 attributable to an even longer delay in PI4P induction and redistribution (**Fig. 6**). GG PV does not produce
348 any 3AB or 3CD, which is likely the cause of this phenotype [42, 43]. This mutant clearly establishes a role
349 for P3 proteins in formation of the replication organelle. However, TEM of GG PV-infected cells revealed
350 a cell full of tubules at times in which genome replication of GG PV RNA was occurring exponentially (**Fig.
351 6**). Hints of tubulation were evident in micrographs of EG and WT PVs (**Figs. 3 and 4**), but tubules never
352 really accumulated. We propose that the tubules observed in GG PV-infected cells are an intermediate
353 on path to formation of the vesicular clusters. Positive invagination of the tubules and interactions
354 between invaginated membranes should produce vesicular clusters, as seen in cross section by TEM. As
355 to function of the vesicular clusters, GG PV was unable to produce significant titers of infectious virus [42,
356 43]. We propose that formation of vesicular clusters requires 3AB and/or 3CD and facilitates virus
357 assembly. It is known that 3CD promotes cell-free synthesis of infectious PV [56, 57]. It is possible that
358 these membranes serve as an assembly organelle.

359 There was a time when poliovirus non-structural proteins were considered in two categories:
360 those that had an impact on interactions with the host; and those that had an impact on genome
361 replication. Emphasis was often placed on shut off of host protein synthesis, permeabilization of cellular
362 membranes and formation of vesicles by P2-encoded proteins. P3-encoded proteins bind to the viral
363 genome, produce the peptide/precursor used to initiate genome replication and function to replicate the
364 genome. This study highlights the almost unlimited functional capacity of PV non-structural proteins by
365 now implicating P3 proteins in events both before and after genome replication. Understanding how
366 these proteins contribute to these events requires further study. It is likely that the findings reported
367 here for PV will apply to other picornaviruses as well.

368 **MATERIALS AND METHODS**

369 **Materials.** Cell culture media and supplements were from Invitrogen Life Technologies (Gibco); Difco-
370 NZCYM for bacterial growth was from BD Biosciences; 5X Cell Culture Lysis Reagent was purchased from
371 Promega; primary antibody against PI4P was purchased from Echelon biosciences; Alexafluor-594-IgM
372 (goat anti-mouse) was from ThermoFisher Scientific; 16% formaldehyde, methanol-free, ultrapure was
373 purchased from polysciences; Digitonin was from Sigma-Aldrich; Bovine Serum Albumin (BSA)-Fraction V,
374 heat shock treated was from Fisher Bioreagents; Vectashield Antifade Mounting Medium with DAPI was
375 from Vector Laboratories; nitrocellulose membrane was from GE Healthcare; TransIT-mRNA transfection
376 kit was purchased from Mirus Bio LLC.

377

378 **Construction of 3B-3C Gly-Gly mutant EGFP subgenomic replicon**. Enhanced green fluorescence protein
379 (EGFP) integrated subgenomic replicon plasmid, pREGFP-, was generated by replacing luciferase gene in
380 pRLuc- [42] with EGFP. PCR was used to amplify the EGFP region using the oligonucleotides NotI-EGFP-
381 for (5'-AAT TCG GAG CGG CCG CTG TGA GCA AGG GCG AGG AGC-3') and EGFP-XhoI-rev (5'-GTC AGA TCC
382 TCG AGC TTG TAC AGC TCG TCC ATG-3') and pEGFP as a template. The PCR product replaced luciferase
383 gene in pRLuc-GG using NotI and XhoI sites to obtain pREGFP-GG subgenomic replicon. Sequencing at the
384 Penn State Nucleic Acid facility was used to confirm all clones.

385

386 **RNA transcription.** Linearization and RNA transcription were performed as described previously [42].
387 Briefly, the pMo-, pRLuc- and pREGFP- plasmids were linearized with EcoRI or ApaI and purified with Qiaex
388 II bead suspension (Qiagen) following manufacture's protocol. RNA was then transcribed from the
389 linearized plasmid DNAs in a 20 µL reaction containing 350 mM HEPES, pH 7.5, 32 mM magnesium acetate,
390 40 mM dithiothreitol (DTT), 2 mM spermidine, 28 mM nucleoside triphosphates (NTPs), 0.025 µg/µL
391 linearized DNA, and 0.025 µg/µL T7 RNA polymerase. The reaction mixture was incubated for 3 h at 37°C
392 and magnesium pyrophosphate was removed by centrifugation for 2 min. The supernatant was
393 transferred to a new tube and subjected to RQ1 DNase treatment (Promega) for 30 min at 37°C. RNA
394 quality was then verified by 0.8% agarose gel electrophoresis. The RNA concentration was determined by
395 comparing pre-known purified RNA side-by-side on an agarose gel.

396

397 **Subgenomic luciferase replicon assay**. Subgenomic luciferase assays were performed as described
398 previously [42] with the following modifications. Subgenomic replicon RNA (5 µg of *in vitro* transcribed
399 RNA) was electroporated into HeLa cells. The cells were incubated in normal growth media (DMEM/F12

400 supplemented with 10% fetal bovine serum, 1% penicillin/streptomycin, 5 mL/1 X 10^6 cells) and 1 X 10^5
401 cells were harvested and lysed using 100 µL of 1X cell culture lysis reagent (CCLR) at an indicated time
402 post-electroporation. Luciferase activity was measured by adding an equal volume of firefly luciferase
403 assay substrate to cell lysate and the reaction mixture was applied to a Junior LB 9509 luminometer
404 (Berthold Technologies) to read relative light units (RLU) for 10 s. Relative light units (RLU) were then
405 normalized based on the total protein concentration determined by Biorad protein assay reagent (BioRad)
406 for each sample. GuHCl when used, the final concentration was 3 mM and the inhibitor was kept on cells
407 during transfection and after, for the entire incubation period.
408
409 **Total RNA preparation**. One day prior to infection, 4 X 10^6 HeLa cells were seeded in a 100 mm dish. On
410 the day of infection, the prepared HeLa monolayers were infected at an MOI 10 with WT or EG PV for 30
411 min at room temperature. Infected cells were washed once with PBS to remove unattached virus and
412 then incubated in normal growth media (DMEM/F12 supplemented with 10% fetal bovine serum and 1%
413 penicillin/streptomycin) at 37°C. At the indicated times post-infection, cells were lysed with 1 mL of Trizol
414 (Invitrogen Life Technologies) and total RNAs were purified by following manufacture's protocol. In order
415 to purify subgenomic replicon RNA containing total RNA, HeLa cells were transfected with subgenomic
416 RNA as described above and 1.2 X 10^6 HeLa cells were lysed with 1 mL Trizol. The RNA quantity was
417 determined using NanoDrop 1000 (ThermoFisher Scientific) and the quality was evaluated by using 0.8%
418 agarose gel.
419
420 **Northern-Blot analysis of RNA synthesis**. Northern-Blot analysis was performed as described previously
421 [43]. Briefly, the RNA was separated on a 0.6% denaturing agarose gel (0.8 M formaldehyde in 1X MOPS)
422 by running at 120V for 2 h. The gel was washed in water for 30 min twice followed by soaking in 20X SSC
423 (Saline Sodium Citrate) buffer for 30 min. RNA was transferred to nylon membrane (Hybond XL, GE
424 Healthcare) using capillary blotting with 20X SSC for 16 h at room temperature. RNA was crosslinked to
425 membrane using UV Crosslinker (Stratalinker 2400, Stratagene). The membrane was washed twice with
426 wash buffer (1X SSC and 0.1% SDS) at 65°C for 30 min each and prehybridized in 100 mL of modified church
427 buffer (0.5 M sodium phosphate, pH 7.2, 7% SDS, and 1 mM EDTA) for 4 h at 65°C. Hybridization was
428 performed in a modified church buffer for 16 h at 65°C. The membrane was washed with wash buffer (1X
429 SSC and 0.1% SDS) for 20 min at 65°C twice and once at room temperature. RNA was visualized by
430 exposing the membrane to a phosphor screen followed by scanning the screen on a Typhoon 8600 scanner
431 (Promega) in phosphor mode. Hybridization probe was made by PCR using oligonucleotides: 3Dseq-100-

432 for (5'-GTT TGA AGG GGT GAA GGA A-3') and 3Dseq-1085-rev (5'-CTC CCA TGT GAC TGT TTC AAA TG-3')
433 and pRLuc-RA as a template. In the reaction, [α-^{32}P]-dATP (1 mCi/mL, 3000 Ci/mmol, GE Healthcare) was
434 used with cold dNTPs (300 µM for each dCTP, dGTP, and dTTP and 10 µM for dATP) in total 100 µl reaction.
435 The quality of PCR product was confirmed by agarose gel electrophoresis and cpm was determined by
436 using scintillation counter (LKB Wallac 1217 Rackbeta liquid scintillation counter).
437
438 **One step growth curve assay.** One day prior to infection, HeLa cells were seeded into 6-well plate at a
439 density of 5 X 10^5 cells/well. On the day of infection, the prepared HeLa monolayers were washed and
440 infected with WT or EG virus at an MOI of 10 for 30 min at room temperature. Infected cells were washed
441 once with PBS to remove unattached virus and then incubated at 37°C. At varying times post-infection,
442 virus was harvested from cells and media by three freeze-thaw cycles with vortexing in between. The
443 isolated virus was quantified by plaque assay.
444
445 **Virus quantification by plaque assay.** For plaque assay, 0.5 X 10^6 HeLa cells were plated one day prior to
446 infection in 6-well plates. On the day of infection, the media was removed and the cells were washed
447 once in PBS. Next, the cells were infected with the 10-fold dilutions of viral supernatants previously
448 prepared and incubated for 30 min at 37°C. The inoculum was then removed and the cells were overlaid
449 with 1% low-melting-point agarose (EMD). The overlay was allowed to solidify for 20 min at room
450 temperature, and the plates were incubated at 37°C for 2 days to allow for plaque formation. 30 min
451 prior to harvesting, the overlays were incubated with 4% formaldehyde/PBS to fix virus and cells. The
452 agarose monolayers were then removed and plaques stained with crystal violet and counted. Viral titers
453 were calculated in PFU/ml.
454
455 **Sorting subgenomic replicon expressing cells with flow cytometer**. WT and GG-subgenomic replicon
456 RNAs (2 µg of *in vitro* transcribed pRLuc RNA and 4 µg of *in vitro* transcribed pREGFP RNA) were
457 electroporated into 1.2 X 10^7 HeLa cells. The cells were incubated in normal growth media at 34°C and
458 luciferase activity was monitored. When the specific activity of luciferase was about 10,000 RLU/µg of
459 total protein (5 h post-transfection for pRLuc-/pREGFP-WT and 14 h post-transfection for pRLuc-/pREGFP-
460 GG), cells were harvested, chilled on ice for 5 min and sorted to collect transfection positive cells. For the
461 sorting, EGFP positive cells were excited with a 488 Argon laser, detected with a 532/40 nm band pass
462 filter and sorted by Cytopeia Influx sorter (Beckton-Dickinson, San Jose, CA) with 100 micron tip at 15 psi.
463 The sorted HeLa cells were processed for transmission electron microscopy.

464 **Transmission electron microscopy**. Virus-Infected HeLa cells or EGFP-positive post-sorted HeLa cells were
465 harvested, fixed and embedded for TEM studies as described previously [43]. Briefly, the harvested cells
466 were fixed with 1% glutaraldehyde, washed with 0.1 M cacodylate (Sodium dimethyl arsenate, Electron
467 Microscopy Sciences) twice for 5 min each, incubated in 1% reduced osmium tetroxide containing 1%
468 potassium ferricyanide in 0.1 M cacodylate for 60 min in the dark with one exchange and washed two
469 times with 0.1 M cacodylate again. En bloc staining was performed with 3% uranyl acetate in 50% ethanol
470 for 60 min in the dark. Dehydration was carried out with different concentrations of ethanol (50, 70, 95
471 and 100% for 5-10 min) and 100% acetonitrile. Embedding was performed overnight with 100% Epon at
472 65ºC. The embedded sample was sectioned with a diamond knife (DiATOME) to slice 60-90 nm thickness
473 by using ultra microtome (Reichart-Jung). The sectioned sample was place on copper grid (Electron
474 Microscopy Science), stained with 2% uranyl acetate in 50% ethanol followed by lead citrate staining for
475 12 min. The grid was washed with H_2O and the grid was dried completely. The image was obtained by
476 using Jeol JEM 1200 EXII and FEI Tecnai G2 Spirit BioTwin located in Electron Microscopy Facility in
477 Pennsylvania State University.
478
479 **Immunofluorescence.** 2.5 X 10^5 cells were seeded on coverslips in 6-well plates and next day infected
480 with WT or EG virus at an MOI of 10. GuHCl whenever used, the final concentration was 3 mM and the
481 inhibitor was kept on cells with the virus for 30 min and for the entire incubation period thereafter. For
482 subgenomic replicon RNA transfection, same number of cells were transfected with 2 µg pREGFP-GG RNA
483 using the RNA transfection kit (Mirus). Infected or transfected cells were fixed with 4% formaldehyde at
484 indicated times post-infection or transfection. Post-fixation, cells were permeabilized with 20 µM
485 digitonin for 10 min and washed with PBS. Cells were then blocked with 3% BSA in PBS for 1 h followed
486 by incubation with anti-PI4P (1:200) antibody for 1 h in blocking buffer. This was followed by washing with
487 PBS and incubating with Alexafluor594; IgM (1:1000) for 1 h. Finally, the cells were washed with PBS and
488 mounted on slides using mounting buffer with DAPI. Samples were imaged with Zeiss Axiovert 200 M
489 epifluorescence microscope.
490
491
492

ACKNOWLEDGMENTS

We thank Dr. Greg Ning and staff of the electron microscopy core facility for their guidance and assistance. This study was funded by grant AI053531 from NIAID, NIH to CEC.

.

AUTHOR CONTRIBUTIONS

Conceptualization: CEC

Funding acquisition: CEC

Investigation: HSO, SB, DAD, JA, MFL

Project administration: HSO, SB, DAD, CEC

Supervision: CEC

Validation: HSO, SB, DAD

Visualization: HSO, SB, DAD

Writing- original draft: HSO, SB, CEC

Writing- review & editing: HSO, SB, JA, CEC

510 **REFERENCES**

511 1. Holmes EC, Drummond AJ. The evolutionary genetics of viral emergence. Curr Top Microbiol Immunol.
512 2007; 315:51-66. Epub 2007/09/13. PMID: 17848060.
513 2. Korboukh VK, Lee CA, Acevedo A, Vignuzzi M, Xiao Y, Arnold JJ, et al. RNA virus population diversity, an
514 optimum for maximal fitness and virulence. J Biol Chem. 2014; 289(43):29531-44. Epub 2014/09/13.
515 https://doi.org/10.1074/jbc.M114.592303 PMID: 25213864.
516 3. Aguilera ER, Erickson AK, Jesudhasan PR, Robinson CM, Pfeiffer JK. Plaques Formed by Mutagenized
517 Viral Populations Have Elevated Coinfection Frequencies. MBio. 2017; 8(2). Epub 2017/03/16.
518 https://doi.org/10.1128/mBio.02020-16 PMID: 28292984.
519 4. Chen YH, Du W, Hagemeijer MC, Takvorian PM, Pau C, Cali A, et al. Phosphatidylserine vesicles enable
520 efficient en bloc transmission of enteroviruses. Cell. 2015; 160(4):619-30. Epub 2015/02/14.
521 https://doi.org/10.1016/j.cell.2015.01.032 PMID: 25679758.
522 5. Robinson CM, Jesudhasan PR, Pfeiffer JK. Bacterial lipopolysaccharide binding enhances virion stability
523 and promotes environmental fitness of an enteric virus. Cell Host Microbe. 2014; 15(1):36-46. Epub
524 2014/01/21. https://doi.org/10.1016/j.chom.2013.12.004 PMID: 24439896.
525 6. den Boon JA, Ahlquist P. Organelle-like membrane compartmentalization of positive-strand RNA virus
526 replication factories. Annu Rev Microbiol. 2010; 64:241-56. Epub 2010/09/10.
527 https://doi.org/10.1146/annurev.micro.112408.134012 PMID: 20825348.
528 7. Belov GA, Sztul E. Rewiring of cellular membrane homeostasis by picornaviruses. J Virol. 2014;
529 88(17):9478-89. Epub 2014/06/13. https://doi.org/10.1128/jvi.00922-14 PMID: 24920802.
530 8. Kallman F, Williams RC, Dulbecco R, Vogt M. Fine structure of changes produced in cultured cells
531 sampled at specified intervals during a single growth cycle of polio virus. J Biophys Biochem Cytol. 1958;
532 4(3):301-8. Epub 1958/05/25. PMID: 13549502.
533 9. Belov GA, Nair V, Hansen BT, Hoyt FH, Fischer ER, Ehrenfeld E. Complex dynamic development of
534 poliovirus membranous replication complexes. J Virol. 2012; 86(1):302-12. Epub 2011/11/11.
535 https://doi.org/10.1128/jvi.05937-11 PMID: 22072780.
536 10. Bienz K, Egger D, Pfister T, Troxler M. Structural and functional characterization of the poliovirus
537 replication complex. J Virol. 1992; 66(5):2740-7. Epub 1992/05/01. PMID: 1313898.
538 11. Bienz K, Egger D, Rasser Y, Bossart W. Kinetics and location of poliovirus macromolecular synthesis in
539 correlation to virus-induced cytopathology. Virology. 1980; 100(2):390-9. Epub 1980/01/30. PMID:
540 6243433.

541 12. Schlegel A, Giddings TH, Jr., Ladinsky MS, Kirkegaard K. Cellular origin and ultrastructure of
542 membranes induced during poliovirus infection. J Virol. 1996; 70(10):6576-88. Epub 1996/10/01. PMID:
543 8794292.
544 13. Troxler M, Egger D, Pfister T, Bienz K. Intracellular localization of poliovirus RNA by in situ hybridization
545 at the ultrastructural level using single-stranded riboprobes. Virology. 1992; 191(2):687-97. Epub
546 1992/12/01. PMID: 1333118.
547 14. Bienz K, Egger D, Troxler M, Pasamontes L. Structural organization of poliovirus RNA replication is
548 mediated by viral proteins of the P2 genomic region. J Virol. 1990; 64(3):1156-63. Epub 1990/03/01.
549 PMID: 2154600.
550 15. Bienz K, Egger D, Pasamontes L. Association of polioviral proteins of the P2 genomic region with the
551 viral replication complex and virus-induced membrane synthesis as visualized by electron microscopic
552 immunocytochemistry and autoradiography. Virology. 1987; 160(1):220-6. Epub 1987/09/01. PMID:
553 2820130.
554 16. Bienz K, Egger D, Rasser Y, Bossart W. Intracellular distribution of poliovirus proteins and the induction
555 of virus-specific cytoplasmic structures. Virology. 1983; 131(1):39-48. Epub 1983/11/01. PMID: 6316654.
556 17. Hsu NY, Ilnytska O, Belov G, Santiana M, Chen YH, Takvorian PM, et al. Viral reorganization of the
557 secretory pathway generates distinct organelles for RNA replication. Cell. 2010; 141(5):799-811. Epub
558 2010/06/01. https://doi.org/10.1016/j.cell.2010.03.050 PMID: 20510927.
559 18. Racaniello VR. Picornaviridae: the viruses and their replication. In: Knipe DM, Howley PM, editors.
560 Fields virology. 6th ed. Philadelphia, PA: Lippincott Williams & Wilkins. p. 453-89
561 19. Cho MW, Teterina N, Egger D, Bienz K, Ehrenfeld E. Membrane rearrangement and vesicle induction
562 by recombinant poliovirus 2C and 2BC in human cells. Virology. 1994; 202(1):129-45. Epub 1994/07/01.
563 https://doi.org/10.1006/viro.1994.1329 PMID: 8009827.
564 20. Teterina NL, Gorbalenya AE, Egger D, Bienz K, Ehrenfeld E. Poliovirus 2C protein determinants of
565 membrane binding and rearrangements in mammalian cells. J Virol. 1997; 71(12):8962-72. Epub
566 1997/11/26. PMID: 9371552.
567 21. Suhy DA, Giddings TH, Jr., Kirkegaard K. Remodeling the endoplasmic reticulum by poliovirus infection
568 and by individual viral proteins: an autophagy-like origin for virus-induced vesicles. J Virol. 2000;
569 74(19):8953-65. Epub 2000/09/12. PMID: 10982339.
570 22. Ventoso I, MacMillan SE, Hershey JW, Carrasco L. Poliovirus 2A proteinase cleaves directly the eIF-4G
571 subunit of eIF-4F complex. FEBS Lett. 1998; 435(1):79-83. Epub 1998/10/02. PMID: 9755863.

572 23. Haghighat A, Svitkin Y, Novoa I, Kuechler E, Skern T, Sonenberg N. The eIF4G-eIF4E complex is the
573 target for direct cleavage by the rhinovirus 2A proteinase. J Virol. 1996; 70(12):8444-50. Epub 1996/12/01.
574 PMID: 8970966.
575 24. Li JP, Baltimore D. An intragenic revertant of a poliovirus 2C mutant has an uncoating defect. J Virol.
576 1990; 64(3):1102-7. Epub 1990/03/01. PMID: 2154595.
577 25. Li JP, Baltimore D. Isolation of poliovirus 2C mutants defective in viral RNA synthesis. J Virol. 1988;
578 62(11):4016-21. Epub 1988/11/01. PMID: 2845120.
579 26. Vance LM, Moscufo N, Chow M, Heinz BA. Poliovirus 2C region functions during encapsidation of viral
580 RNA. J Virol. 1997; 71(11):8759-65. Epub 1997/10/29. PMID: 9343235.
581 27. Liu Y, Wang C, Mueller S, Paul AV, Wimmer E, Jiang P. Direct interaction between two viral proteins,
582 the nonstructural protein 2C and the capsid protein VP3, is required for enterovirus morphogenesis. PLoS
583 Pathog. 2010; 6(8):e1001066. Epub 2010/09/25. https://doi.org/10.1371/journal.ppat.1001066 PMID:
584 20865167.
585 28. Asare E, Mugavero J, Jiang P, Wimmer E, Paul AV. A Single Amino Acid Substitution in Poliovirus
586 Nonstructural Protein 2CATPase Causes Conditional Defects in Encapsidation and Uncoating. J Virol. 2016;
587 90(14):6174-86. Epub 2016/04/15. https://doi.org/10.1128/jvi.02877-15 PMID: 27076638.
588 29. Pincus SE, Diamond DC, Emini EA, Wimmer E. Guanidine-selected mutants of poliovirus: mapping of
589 point mutations to polypeptide 2C. J Virol. 1986; 57(2):638-46. Epub 1986/02/01. PMID: 3003395.
590 30. Baltera RF, Jr., Tershak DR. Guanidine-resistant mutants of poliovirus have distinct mutations in
591 peptide 2C. J Virol. 1989; 63(10):4441-4. Epub 1989/10/01. PMID: 2550675.
592 31. Hope DA, Diamond SE, Kirkegaard K. Genetic dissection of interaction between poliovirus 3D
593 polymerase and viral protein 3AB. J Virol. 1997; 71(12):9490-8. Epub 1997/11/26. PMID: 9371611.
594 32. Giachetti C, Hwang SS, Semler BL. cis-acting lesions targeted to the hydrophobic domain of a poliovirus
595 membrane protein involved in RNA replication. J Virol. 1992; 66(10):6045-57. Epub 1992/10/01. PMID:
596 1326655.
597 33. Andino R, Rieckhof GE, Achacoso PL, Baltimore D. Poliovirus RNA synthesis utilizes an RNP complex
598 formed around the 5'-end of viral RNA. Embo j. 1993; 12(9):3587-98. Epub 1993/09/01. PMID: 8253083.
599 34. Gamarnik AV, Andino R. Switch from translation to RNA replication in a positive-stranded RNA virus.
600 Genes Dev. 1998; 12(15):2293-304. Epub 1998/08/08. PMID: 9694795.
601 35. Parsley TB, Towner JS, Blyn LB, Ehrenfeld E, Semler BL. Poly (rC) binding protein 2 forms a ternary
602 complex with the 5'-terminal sequences of poliovirus RNA and the viral 3CD proteinase. Rna. 1997;
603 3(10):1124-34. Epub 1997/11/05. PMID: 9326487.

604 36. Paul AV, Rieder E, Kim DW, van Boom JH, Wimmer E. Identification of an RNA hairpin in poliovirus
605 RNA that serves as the primary template in the in vitro uridylylation of VPg. J Virol. 2000; 74(22):10359-
606 70. Epub 2000/10/24. PMID: 11044080.
607 37. Rieder E, Paul AV, Kim DW, van Boom JH, Wimmer E. Genetic and biochemical studies of poliovirus
608 cis-acting replication element cre in relation to VPg uridylylation. J Virol. 2000; 74(22):10371-80. Epub
609 2000/10/24. PMID: 11044081.
610 38. Toyoda H, Nicklin MJ, Murray MG, Anderson CW, Dunn JJ, Studier FW, et al. A second virus-encoded
611 proteinase involved in proteolytic processing of poliovirus polyprotein. Cell. 1986; 45(5):761-70. Epub
612 1986/06/06. PMID: 3011278.
613 39. Nicklin MJ, Harris KS, Pallai PV, Wimmer E. Poliovirus proteinase 3C: large-scale expression,
614 purification, and specific cleavage activity on natural and synthetic substrates in vitro. J Virol. 1988;
615 62(12):4586-93. Epub 1988/12/01. PMID: 2846872.
616 40. Ypma-Wong MF, Semler BL. In vitro molecular genetics as a tool for determining the differential
617 cleavage specificities of the poliovirus 3C proteinase. Nucleic Acids Res. 1987; 15(5):2069-88. Epub
618 1987/03/11. PMID: 3031587.
619 41. Lawson MA, Semler BL. Alternate poliovirus nonstructural protein processing cascades generated by
620 primary sites of 3C proteinase cleavage. Virology. 1992; 191(1):309-20. Epub 1992/11/01. PMID:
621 1329322.
622 42. Pathak HB, Oh HS, Goodfellow IG, Arnold JJ, Cameron CE. Picornavirus genome replication: roles of
623 precursor proteins and rate-limiting steps in oriI-dependent VPg uridylylation. J Biol Chem. 2008;
624 283(45):30677-88. Epub 2008/09/10. https://doi.org/10.1074/jbc.M806101200 PMID: 18779320.
625 43. Oh HS, Pathak HB, Goodfellow IG, Arnold JJ, Cameron CE. Insight into poliovirus genome replication
626 and encapsidation obtained from studies of 3B-3C cleavage site mutants. J Virol. 2009; 83(18):9370-87.
627 Epub 2009/07/10. https://doi.org/10.1128/jvi.02076-08 PMID: 19587035.
628 44. Towner JS, Mazanet MM, Semler BL. Rescue of defective poliovirus RNA replication by 3AB-containing
629 precursor polyproteins. J Virol. 1998; 72(9):7191-200. Epub 1998/08/08. PMID: 9696813.
630 45. Jurgens C, Flanegan JB. Initiation of poliovirus negative-strand RNA synthesis requires precursor forms
631 of p2 proteins. J Virol. 2003; 77(2):1075-83. Epub 2002/12/28. PMID: 12502823.
632 46. Novak JE, Kirkegaard K. Coupling between genome translation and replication in an RNA virus. Genes
633 Dev. 1994; 8(14):1726-37. Epub 1994/07/15. PMID: 7958852.

634 47. Wessels E, Duijsings D, Niu TK, Neumann S, Oorschot VM, de Lange F, et al. A viral protein that blocks
635 Arf1-mediated COP-I assembly by inhibiting the guanine nucleotide exchange factor GBF1. Dev Cell. 2006;
636 11(2):191-201. Epub 2006/08/08. https://doi.org/10.1016/j.devcel.2006.06.005 PMID: 16890159.
637 48. Wessels E, Duijsings D, Lanke KH, van Dooren SH, Jackson CL, Melchers WJ, et al. Effects of
638 picornavirus 3A Proteins on Protein Transport and GBF1-dependent COP-I recruitment. J Virol. 2006;
639 80(23):11852-60. Epub 2006/09/29. https://doi.org/10.1128/jvi.01225-06 PMID: 17005635.
640 49. Belov GA, Altan-Bonnet N, Kovtunovych G, Jackson CL, Lippincott-Schwartz J, Ehrenfeld E. Hijacking
641 components of the cellular secretory pathway for replication of poliovirus RNA. J Virol. 2007; 81(2):558-
642 67. Epub 2006/11/03. https://doi.org/10.1128/jvi.01820-06 PMID: 17079330.
643 50. Doedens JR, Kirkegaard K. Inhibition of cellular protein secretion by poliovirus proteins 2B and 3A.
644 Embo j. 1995; 14(5):894-907. Epub 1995/03/01. PMID: 7889939.
645 51. Doedens JR, Giddings TH, Jr., Kirkegaard K. Inhibition of endoplasmic reticulum-to-Golgi traffic by
646 poliovirus protein 3A: genetic and ultrastructural analysis. J Virol. 1997; 71(12):9054-64. Epub
647 1997/11/26. PMID: 9371562.
648 52. Choe SS, Dodd DA, Kirkegaard K. Inhibition of cellular protein secretion by picornaviral 3A proteins.
649 Virology. 2005; 337(1):18-29. Epub 2005/05/26. https://doi.org/10.1016/j.virol.2005.03.036 PMID:
650 15914217.
651 53. Wang J, Ptacek JB, Kirkegaard K, Bullitt E. Double-membraned liposomes sculpted by poliovirus 3AB
652 protein. J Biol Chem. 2013; 288(38):27287-98. Epub 2013/08/03.
653 https://doi.org/10.1074/jbc.M113.498899 PMID: 23908350.
654 54. Belov GA, Habbersett C, Franco D, Ehrenfeld E. Activation of cellular Arf GTPases by poliovirus protein
655 3CD correlates with virus replication. J Virol. 2007; 81(17):9259-67. Epub 2007/06/15.
656 https://doi.org/10.1128/jvi.00840-07 PMID: 17567696.
657 55. Belov GA, Fogg MH, Ehrenfeld E. Poliovirus proteins induce membrane association of GTPase ADP-
658 ribosylation factor. J Virol. 2005; 79(11):7207-16. Epub 2005/05/14.
659 https://doi.org/10.1128/jvi.79.11.7207-7216.2005 PMID: 15890959.
660 56. Franco D, Pathak HB, Cameron CE, Rombaut B, Wimmer E, Paul AV. Stimulation of poliovirus synthesis
661 in a HeLa cell-free in vitro translation-RNA replication system by viral protein 3CDpro. J Virol. 2005;
662 79(10):6358-67. Epub 2005/04/29. https://doi.org/10.1128/jvi.79.10.6358-6367.2005 PMID: 15858019.
663 57. Franco D, Pathak HB, Cameron CE, Rombaut B, Wimmer E, Paul AV. Stimulation of poliovirus RNA
664 synthesis and virus maturation in a HeLa cell-free in vitro translation-RNA replication system by viral

665 protein 3CDpro. Virol J. 2005; 2:86. Epub 2005/11/23. https://doi.org/10.1186/1743-422x-2-86 PMID:
666 16300678.

667 **FIGURE LEGENDS**

668 Figure 1**. Poliovirus genome organization and P3-polyprotein processing.** (**A**) Schematic of the poliovirus
669 genome. The 7.5 kb long genome consists of a 5'-nontranslated region (NTR), an open reading frame, a
670 3'-NTR and a poly(rA) tail. The 5'-end of the genome is covalently linked to a peptide (VPg) encoded by
671 the 3B gene. The 5'-NTR contains a cis-acting replication element (CRE) termed oriL or cloverleaf followed
672 by a type II internal ribosome entry site (IRES). Two additional CREs exist: oriI and oriR, located within the
673 2C gene and 3'-NTR, respectively. IRES mediated translation yields a single polyprotein comprise of three
674 functional domains of structural (P1) and the non-structural (P2 and P3) proteins. (**B**) Processing of the P3
675 region by WT and mutant PVs. Two pathways, major and minor, exist for P3 processing. Major pathway
676 use for WT PV is shown and produces only 3AB and 3CD because of cleavage at Gln-Gly junction between
677 3B and 3C. EG PV changes the 3B-3C junction to Glu-Gly, producing the normal products at a reduced
678 rate. GG PV changes the 3B-3C junction to Gly-Gly, which is uncleavable, inducing aberrant processing
679 and producing 3ABC and 3D instead 3AB and 3CD.

680 Figure 2**. EG PV exhibits a delay in the onset of RNA synthesis.** (**A**) Kinetics of replication of subgenomic
681 replicon by WT (■) and EG (□) monitored indirectly by luciferase activity. HeLa cells were transfected with
682 *in vitro* transcribed replicon RNA, placed at 37 °C and luciferase activity (RLU/µg) measured at the
683 indicated times post-transfection. A control for translation of transfected replicon RNA was performed by
684 performing the experiment above in the presence of 3 Mm GuHCl (●). (**B**) Kinetics of replication of
685 subgenomic replicon by WT (●) and EG (○) monitored by Northern blotting. HeLa cells were transfected
686 with *in vitro* transcribed replicon RNA, placed at 37 °C, and at the indicated times post-transfection, cells
687 were harvested for total RNA isolation. Total RNA was separated on a 0.6% agarose gel containing 0.8 M
688 formaldehyde, transferred to nylon membrane and hybridized with a ^{32}P-labeled DNA probe. (**C**) Image of
689 a representative blot visualized by phosphorimaging. *In vitro* transcribed RNA (*****) is shown as reference.

690 Figure 3**. Kinetics of genome replication precedes the kinetics of vesicular cluster formation for EG PV.**
691 (**A**) Kinetics of RNA synthesis (○) and virus production (●) by EG PV. HeLa cells were infected with EG PV
692 at an MOI of 10, placed at 37 °C, and at the indicated times post-infection, total RNA was isolated and
693 subjected to either Northern blotting or assayed for virus production by standard plaque assay. (**B**) Image
694 of a representative blot visualized by phosphorimaging. **(C)** Kinetics of formation of virus-induced vesicular
695 clusters by transmission electron microscope (TEM). HeLa cells were infected with EG PV at MOI of 10,
696 placed at 37 °C, and at the indicated times post-infection, infected cells were fixed and visualized by TEM,
697 bar = 1 µm.

698 Figure 4. **Kinetics of genome replication precedes the kinetics of vesicular cluster formation for WT PV.**
699 (**A**) Kinetics of RNA synthesis (○) and virus production (●) by WT PV. HeLa cells were infected with WT PV
700 at an MOI of 10, placed at 37 °C, and at the indicated times post-infection, total RNA was isolated and
701 subjected to either Northern blotting or assayed for virus production by standard plaque assay. (**B**) Image
702 of a representative blot visualized by phosphorimaging. (**C**) Kinetics of formation of WT PV-induced
703 vesicular cluster formation was visualized by TEM. HeLa cells were infected with WT PV at an MOI of 10,
704 placed at 37 °C, and at the indicated times post-infection, the infected cells were fixed and visualized by
705 TEM, bar = 1 µm.

706 Figure 5. **EG PV exhibits delayed induction and redistribution of PI4P. (A)** Immunostaining of PI4P in
707 mock-infected HeLa cells. **(B)** Time-course of PI4P-staining in HeLa cells infected with WT or EG PV. HeLa
708 cells were infected with WT or EG virus at an MOI of 10, fixed at indicated times post-infection, and
709 immunostained for PI4P. **(C)** Impact of GuHCl on PI4P induction by WT and EG PVs. HeLa cells were either
710 incubated with PBS or infected with WT or EG virus (MOI 10) in presence of 3 mM GuHCl and
711 immunostained. In all cases, PI4P was stained using anti-PI4P antibody (red) and nuclei were stained with
712 DAPI (blue).

713 Figure 6**. GG PV induces and redistributes PI4P in spite of impaired formation of vesicular clusters.** (**A**)
714 Kinetics of RNA synthesis by WT (●) and GG (Δ) subgenomic replicon RNA. HeLa cells were co-transfected
715 with two different replicon RNAs, luciferase replicon (2 µg) and EGFP replicon (4 µg), placed at 34 °C and
716 at the indicated times post-transfection, luciferase activity was measured. (**B**) Cell sorting to isolate PV
717 replicon-positive cells. WT replicon RNA-transfected cells were 61% positive in pre-sort cells (top-left) and
718 98% positive in post-sort cells (bottom-left). GG replicon RNA transfected cells were 18% positive in pre-
719 sort cells (top-right) and 94% positive in post-sort cells (bottom-right). (**C**) WT and GG PV-induced
720 membranes visualized by TEM. HeLa cells were transfected with either WT or GG replicon RNA, placed at
721 34 °C for 5 h or 14 h, respectively, at which time cells were fixed and visualized by TEM. Bar =1 µm. **(D)**
722 Kinetics of PI4P induction and redistribution by the GG PV subgenomic replicon. HeLa cells were
723 transfected with replicon RNA expressing EGFP and samples were fixed at the indicated time post-
724 transfection and subjected to IFM using anti-PI4P antibody (red) and nuclei were stained with DAPI (blue).

725 Figure 7**. Multiplicity of infection exaggerates size and quantity of WT PV-induced vesicular clusters.**
726 Transmission electron micrographs (TEM) of HeLa cells infected with WT PV at an MOI of 10 **(A),** 50 **(B)** or
727 100 **(C)**. HeLa cells were infected with WT PV expressing EGFP at an MOI of 10, 50 or 100 by incubating
728 the monolayer with WT virus for 30 min at room temperature, followed by removal of the virus and

729 washing of the monolayer with PBS. Prewarmed media was then added to the monolayer and incubated
730 at 37 °C. Samples were fixed 3 h post-infection and visualized by TEM. Bar = 1 µm.

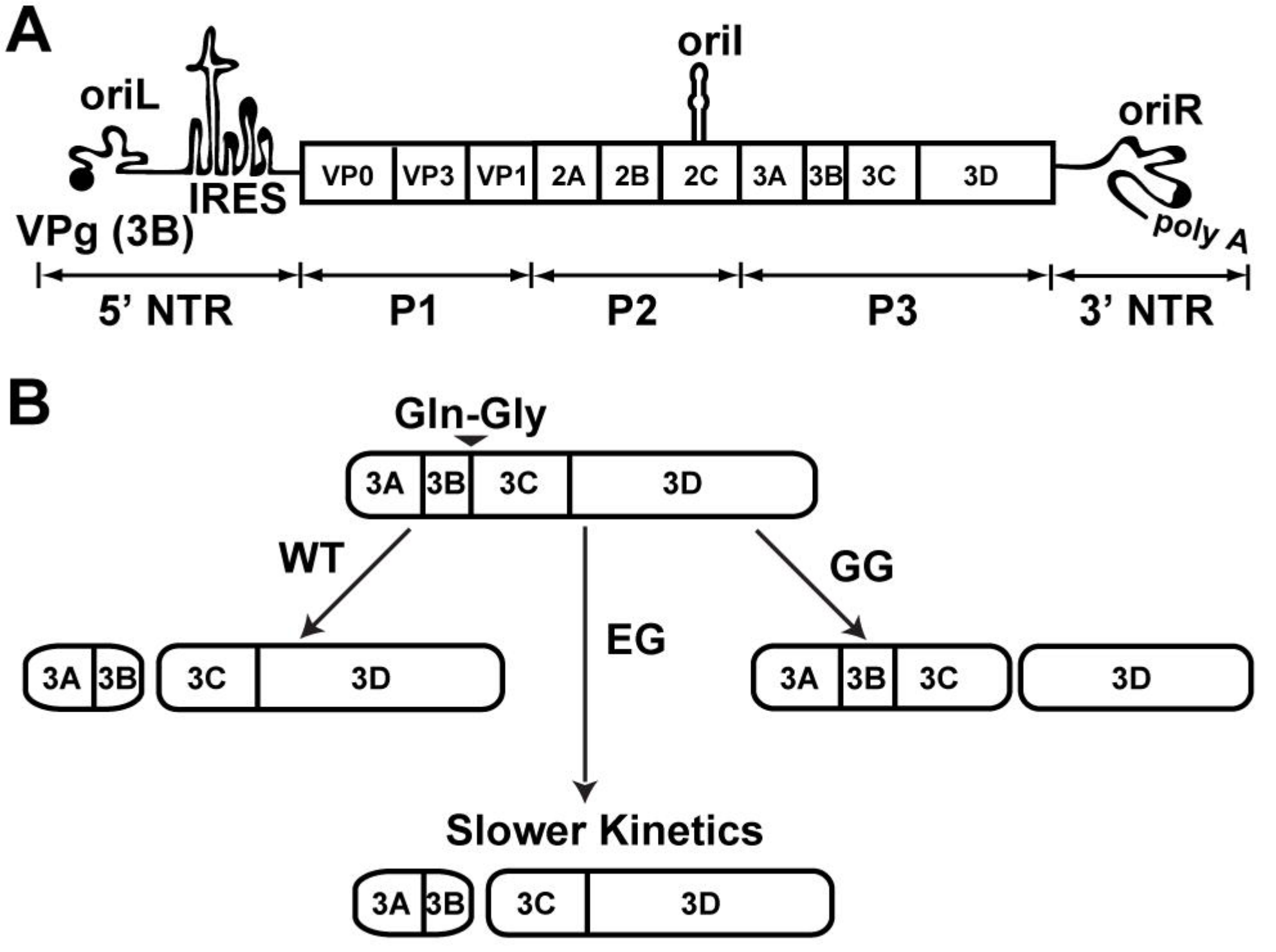
A
oriL
oriI
oriR
IRES
VPg (3B)
VP0
VP3
VP1
2A
2B
2C
3A
3B
3C
3D
poly A
5' NTR
P1
P2
P3
3' NTR
B
Gln-Gly
3A
3B
3C
3D
WT
GG
EG
Slower Kinetics

A

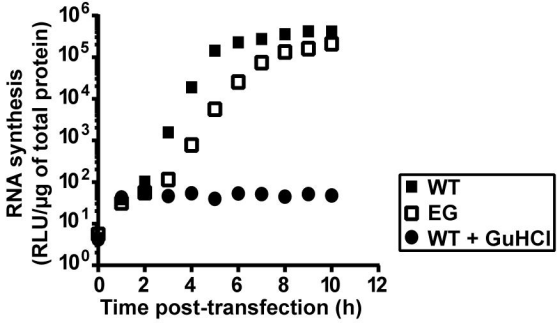

B

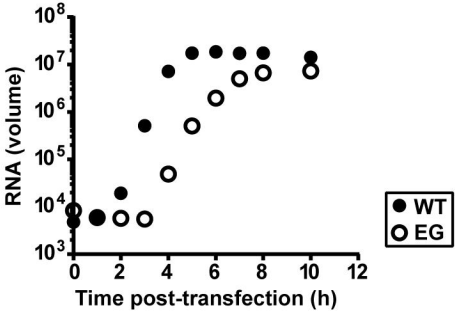

C

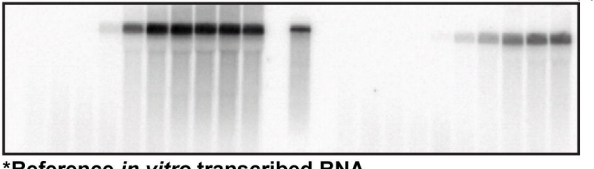

*Reference *in vitro* transcribed RNA

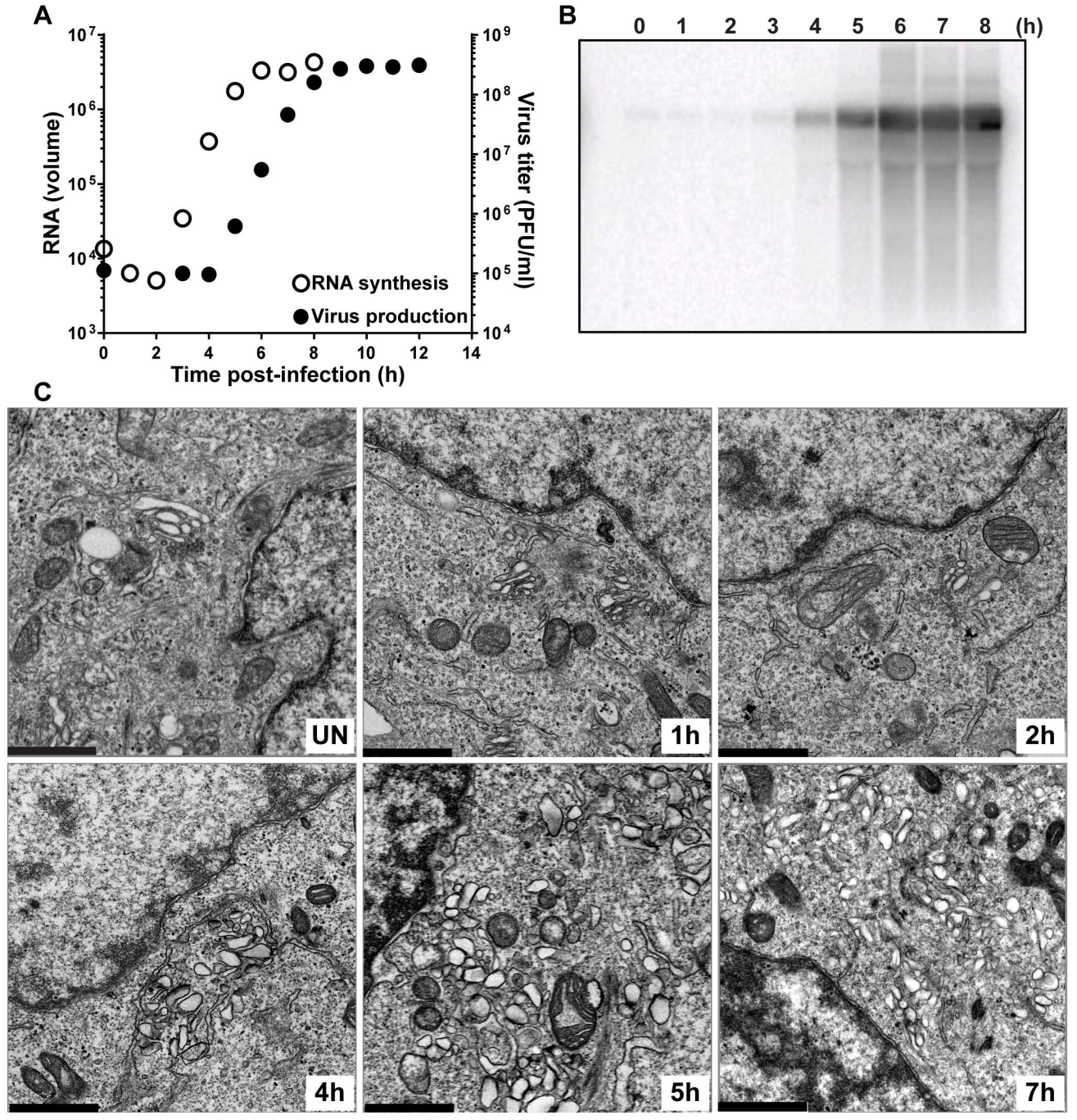
A
RNA (volume)
Virus titer (PFU/ml)
Time post-infection (h)
RNA synthesis
Virus production
B
0 1 2 3 4 5 6 7 8 (h)
C
UN
1h
2h
4h
5h
7h

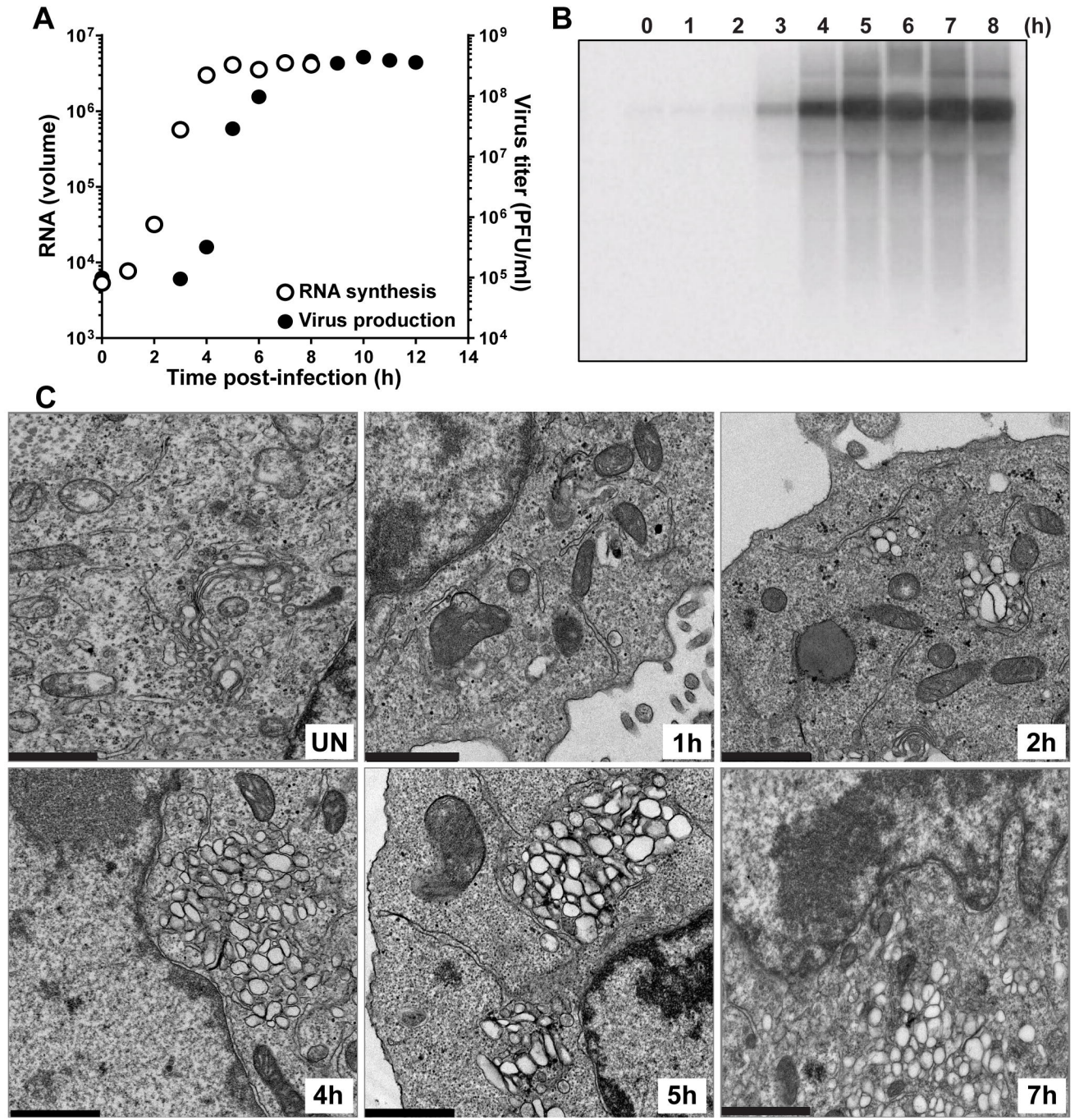
A
RNA (volume)
Virus titer (PFU/ml)
Time post-infection (h)
RNA synthesis
Virus production
B
0 1 2 3 4 5 6 7 8 (h)
C
UN
1h
2h
4h
5h
7h

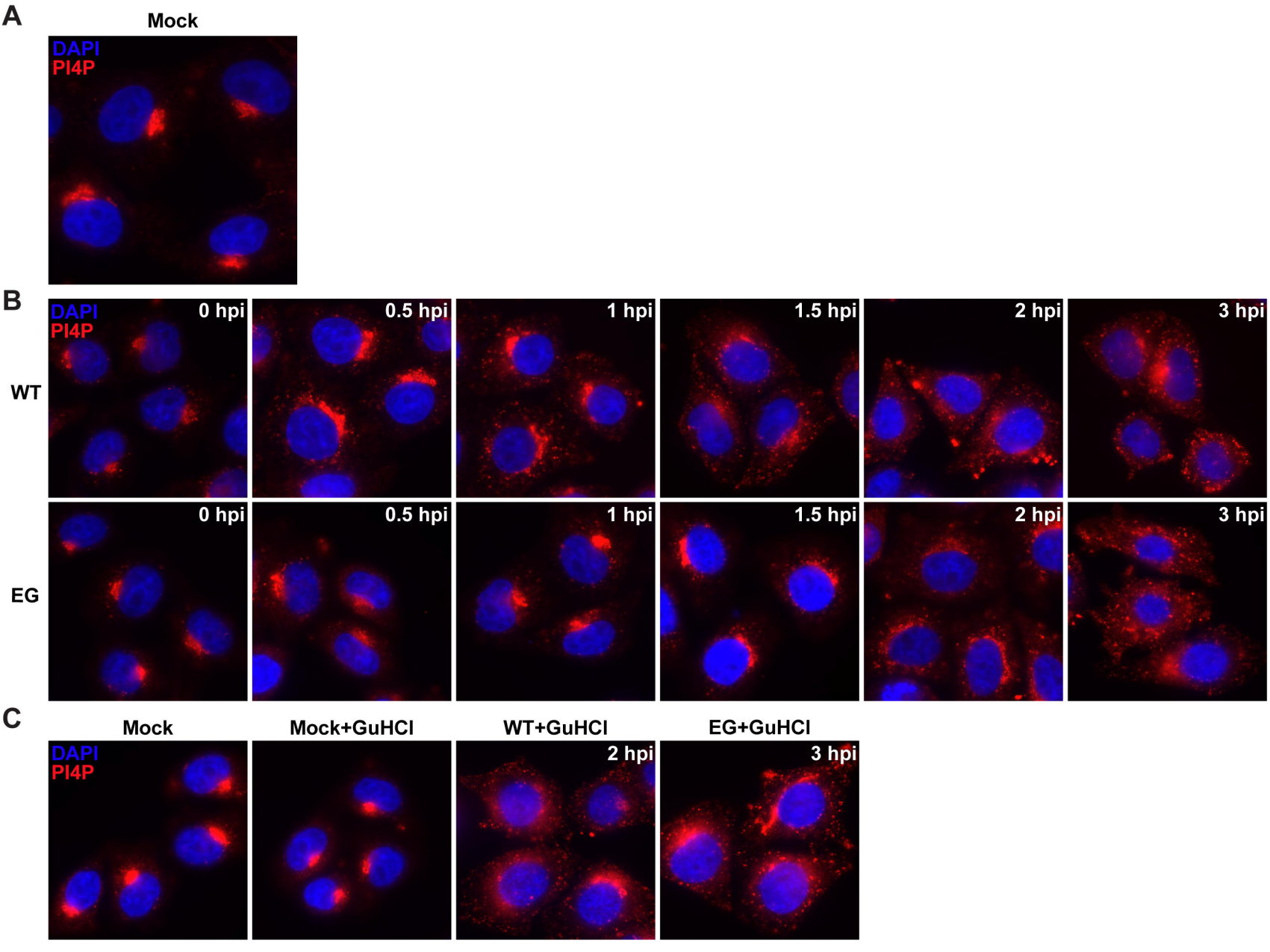
A
Mock
DAPI
PI4P
B
WT
EG
0 hpi
0.5 hpi
1 hpi
1.5 hpi
2 hpi
3 hpi
C
Mock
Mock+GuHCl
WT+GuHCl
EG+GuHCl
2 hpi
3 hpi

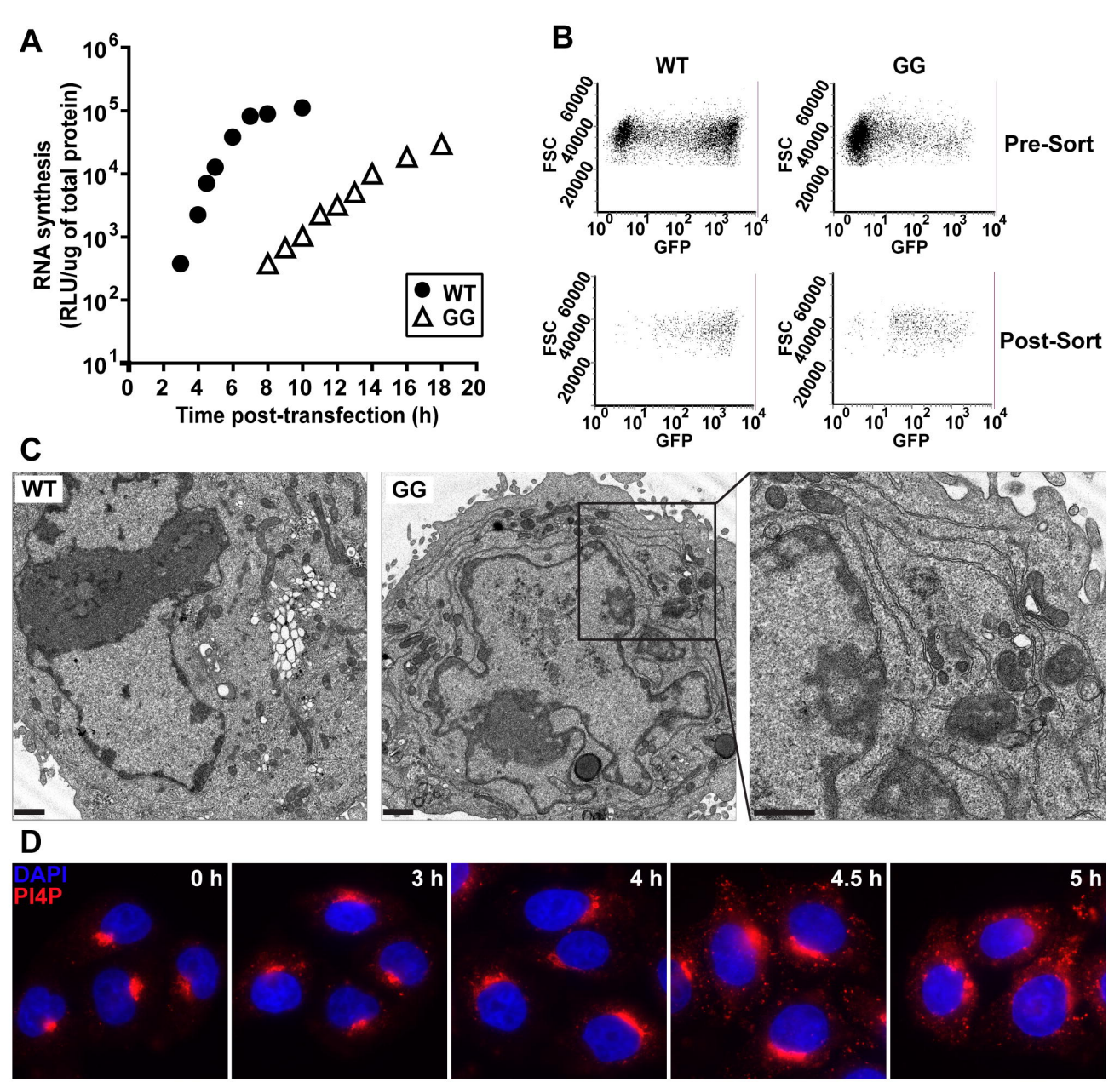
A
RNA synthesis
(RLU/ug of total protein)
Time post-transfection (h)
WT
GG
B
WT
GG
FSC
GFP
Pre-Sort
Post-Sort
C
WT
GG
D
DAPI
PI4P
0 h
3 h
4 h
4.5 h
5 h

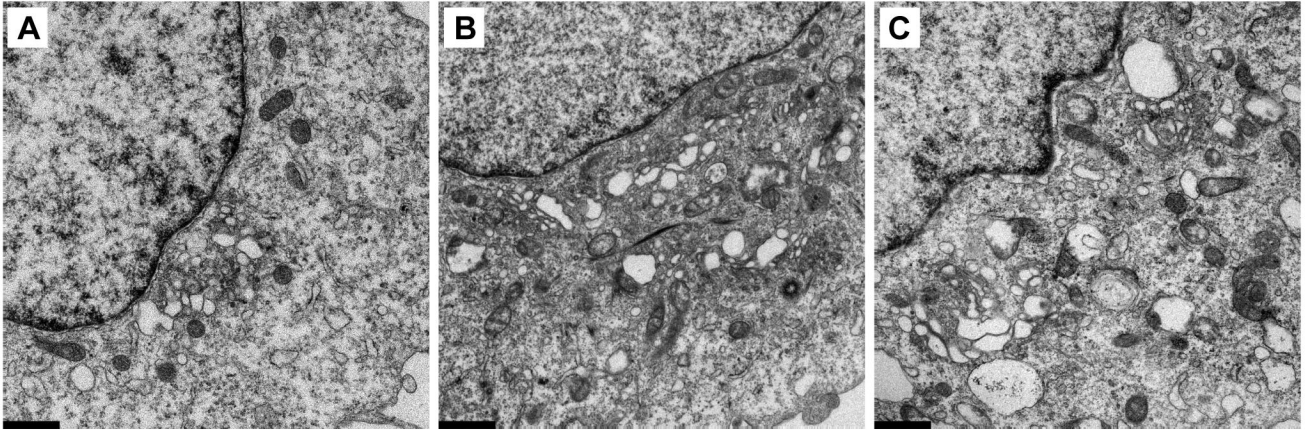
A
B
C